Materialwiss. Werkstofftech. **2022**, *53*, 422–439 doi.org/10.1002/mawe.202100341

Calibration of a combined isotropic-kinematic hardening material model for the simulation of thin electrical steel sheets subjected to cyclic loading

Kalibrierung eines Materialmodells für die Simulation von zyklisch beanspruchten dünnen Elektroblechen unter Berücksichtigung kombinierter isotroper-kinematischer Verfestigung

P. Kubaschinski[1], A. Gottwalt[1], U. Tetzlaff[1], H. Altenbach[2], M. Waltz[1]

The combined isotropic-kinematic hardening model enables the description of the cyclic transient elastic-plastic material behaviour of steel. However, the determination of the material model parameters and understanding of their influence on the material response can be a challenging task. This study deals with the individual steps of the material model calibration for the simulation of thin electrical steel sheets under cyclic loading. Specific recommendations are made for the determination of kinematic and isotropic hardening material parameters. In particular, the isotropic hardening evolution is described by Voce's exponential law and a simple multilinear approach. Based on the multilinear approach, which allows for different slopes in the evolution of the yield surface size, an alternative calibration of the isotropic hardening component is proposed. As a result, the presence of the yield plateau in the first half cycle can be accurately captured, while convergence issues in the material model definition for numerical simulations can be avoided. The comparison of simulated load cycles with experimental cyclic tests shows a good agreement, which indicates the suitability of the proposed material model calibration for electrical steel.

Keywords: Cyclic plasticity **/** material model **/** combined hardening **/** finite-element simulation **/** electrical steel

Die Berücksichtigung kombinierter isotroper-kinematischer Verfestigung ermöglicht die Beschreibung und Modellierung des transienten elastisch-plastischen Werkstoffverhaltens von Stahl. Die Ermittlung der zugrunde liegenden Materialparameter und das Verständnis für deren Einfluss auf die Materialantwort stellt jedoch häufig eine anspruchsvolle Aufgabe dar. In der vorliegenden Arbeit wird auf die einzelnen Schritte bei der Kalibrierung des Materialmodells im Rahmen einer Simulation von zyklisch beanspruchten dünnen Elektroblechen eingegangen. Dabei werden konkrete Empfehlungen für die Ermittlung der kinematischen und isotropen Verfestigungsparameter gegeben. Die Evolutionsgleichung der isotropen Verfestigung wird sowohl durch einen Exponentialansatz nach Voce als auch

[1] Technische Hochschule Ingolstadt, Kompetenzfeld Werkstoff- und Oberflächentechnik, Ingolstadt, Germany
[2] Otto-von-Guericke-Universität Magdeburg, Institut für Mechanik, Magdeburg, Germany

Corresponding author: P. Kubaschinski, Technische Hochschule Ingolstadt, Kompetenzfeld Werkstoff- und Oberflächentechnik, Esplanade 10, 85049, Ingolstadt, Germany,
E-Mail: Paul.Kubaschinski@thi.de

This is an open access article under the terms of the Creative Commons Attribution Non-Commercial NoDerivs License, which permits use and distribution in any medium, provided the original work is properly cited, the use is non-commercial and no modifications or adaptations are made.
© 2022 The Authors. Materialwissenschaft und Werkstofftechnik published by Wiley-VCH GmbH

durch einen einfachen multilinearen Ansatz beschrieben. Basierend auf dem multilinearen Ansatz, der unterschiedliche Steigungen in der Evolution der Fließfläche ermöglicht, wird eine alternative Kalibrierung der isotropen Komponente vorgeschlagen. Dadurch kann das auftretende Fließplateau im ersten Halbzyklus präzise erfasst werden, während Konvergenzprobleme des Materialmodells vermieden werden. Der Vergleich von simulierten Belastungszyklen mit experimentellen Daten zeigt eine gute Übereinstimmung, was für die Eignung des vorgeschlagenen Kalibrierungsprozesses für Elektroblech spricht.

Schlüsselwörter: Zyklische Plastizität / Materialmodell / kombinierte Verfestigung / Finite-Elemente-Simulation / Elektroblech

1 Introduction

The rotor of an electric drive, which consists of several electrical steel sheets, is exposed to high rotational speeds ($\sim 20.000\ \mathrm{min}^{-1}$) and cyclic loading due to acceleration and deceleration. With typical sheet thicknesses of only 0.3 mm, the electrical steel sheets locally exhibit high mechanical stresses and strains. In the context of an analytical fatigue life assessment, the cyclic elastic-plastic material behaviour is evaluated. For this purpose, a suitable, calibrated material model is required.

In recent years, different constitutive models and theories describing the phenomenological mechanisms of cyclic plasticity have been developed and further improved. An overview of several single yield surface models including the respective evolution equations can be viewed in the literature [1]. The choice of the material model for industrial applications, however, can be a challenging task considering model complexity, computation time and experimental data available for the calibration [2].

In this study, the combined isotropic-kinematic hardening model according to Lemaitre and Chaboche is used to describe the transient cyclic elastic-plastic behaviour of electrical steel [3]. It is well-established and implemented in most commercial finite-element applications. The combination of isotropic and kinematic hardening allows for an accurate representation of complex cyclic phenomena, e. g., cyclic softening/hardening and cyclic creep. To ensure a satisfactory alignment between simulation and actual material behaviour, the material parameters have to be carefully determined based on experimental data.

The present work is supposed to give an overview of the constitutive modelling of cyclic plasticity followed by a specific explanation of the material model calibration for electrical steel. Symmetric strain-controlled cyclic tests are performed to provide stress-strain hysteresis curves for the material parameter determination. To avoid buckling of the thin electrical steel sheets under compressive forces, the application of an anti-buckling device is necessary which is described more detailed in this paper. After that, the individual steps of the material parameter determination for the kinematic and isotropic hardening evolution equations are presented.

Numerical simulations are performed in Abaqus comparing the predicted elastic-plastic material behaviour with experimental cyclic tests. The combined isotropic-kinematic hardening model is validated considering cyclic loading both under strain- and stress-control. As a result, the suitability of the determined material parameters can be evaluated.

2 Constitutive modelling of cyclic plasticity: theoretical background

2.1 Cyclic material behaviour of steel

The cyclic material behaviour of steel can be characterised by certain phenomenological mechanisms, which have to be accounted for in the constitutive modelling of cyclic plasticity. Typically, this includes the Bauschinger effect. Under uniaxial cyclic loading, the yield strength $\sigma|_0$ of a specimen decreases, after the loading direction is reversed, *Figure 1*. Considering the first cycle of a symmetric strain-controlled fatigue test, it can be observed that the elastic limit while unloading corresponds to the double of the initial yield strength $2\sigma|_0$.

© 2022 The Authors. Materialwissenschaft und Werkstofftechnik published by Wiley-VCH GmbH

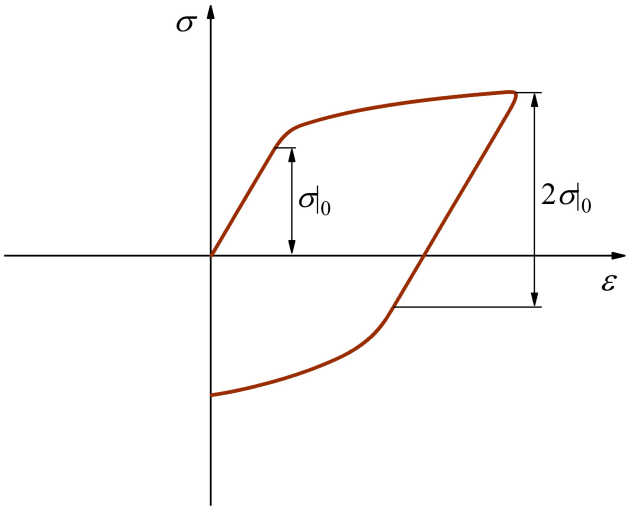

Figure 1. Influence of the Bauschinger effect on the yield strength.

Bild 1. Einfluss des Bauschingereffektes auf die Streckgrenze.

The stress or strain response of a material under cyclic loading can change due to microstructural effects, which results in a decreasing or increasing deformation resistance [1]. This cyclic softening or hardening behaviour is material-specific and depends on the loading amplitude as well as the strain history. The transient material response caused by cyclic softening/hardening under symmetric strain-control is associated with changing stress amplitudes, *Figure 2*. It is usually assumed that the intensity of the response decreases and a stabilised state is reached.

For unsymmetric load cycles under stress-control, ratchetting (cyclic creep) has to be considered, *Figure 3*a. In the case of uniaxial loading, it can be measured as accumulation of axial plastic strain [1]. The ratchetting rate depends on the cyclic softening/hardening and the magnitude of mean stress. In contrast, unsymmetric cycles under strain-control result in mean stress relaxation, Figure 3b.

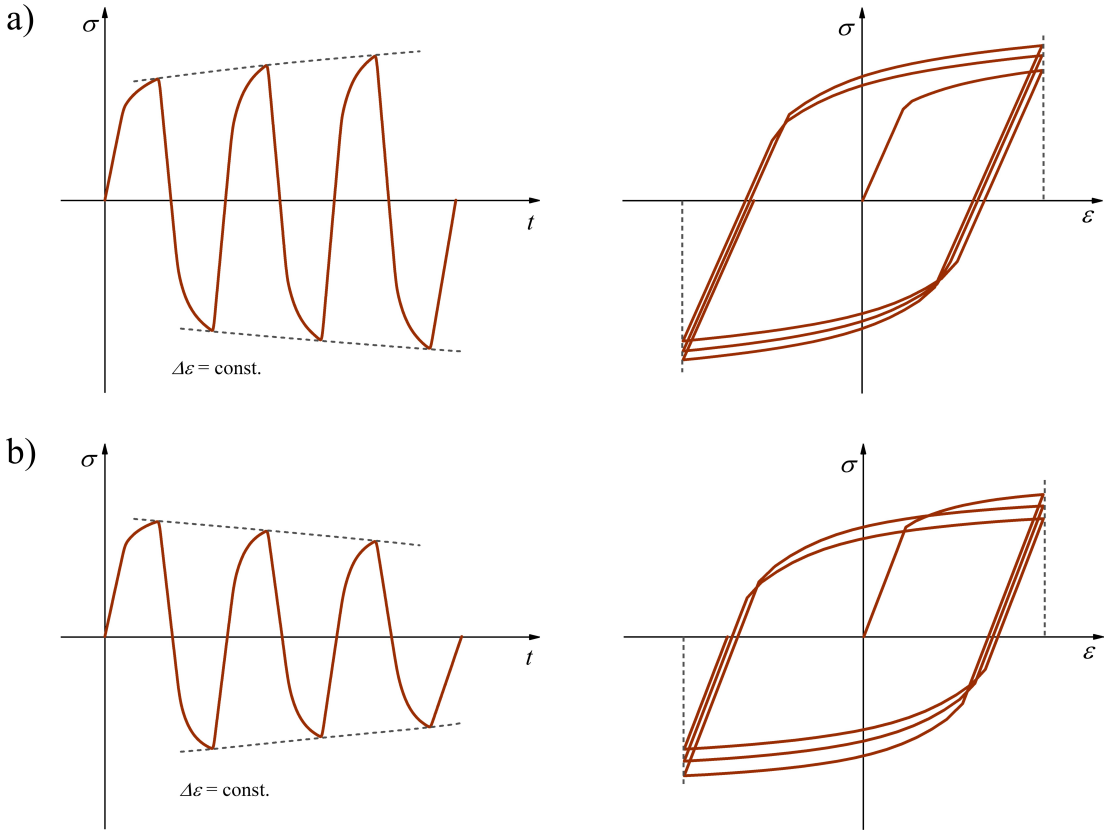

Figure 2. Stress-strain response under symmetric strain-controlled cyclic loading, a) cyclic hardening, b) cyclic softening.

Bild 2. Spannungs-Dehnungsantworten bei symmetrischer dehnungskontrollierter zyklischer Belastung, a) zyklische Verfestigung, b) zyklische Entfestigung.

© 2022 The Authors. Materialwissenschaft und Werkstofftechnik published by Wiley-VCH GmbH

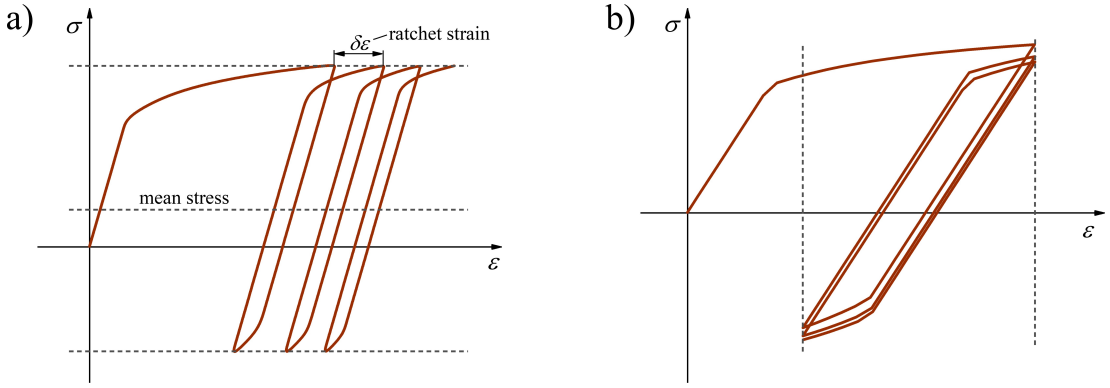

Figure 3. Stress-strain behaviour under unsymmetric cyclic loading, a) ratchetting, b) mean stress relaxation.

Bild 3. Spannungs-Dehnungsverhalten bei unsymmetrischer zyklischer Beanspruchung, a) zyklisches Kriechen, b) Mittelspannungsrelaxation.

With increasing number of cycles, the mean stress tends to approach zero.

Besides the mentioned phenomena, the presence of the yield plateau (Lüders bands propagation) in the first half cycle has to be given particular consideration. It can be idealised as a non-hardening region between the yield strain ε_y and the onset of strain hardening ε_{sh}, *Figure 4* [4]. As long as the onset of the strain hardening is not reached, the yield stress remains more or less constant. After load reversal, the yield plateau disappears.

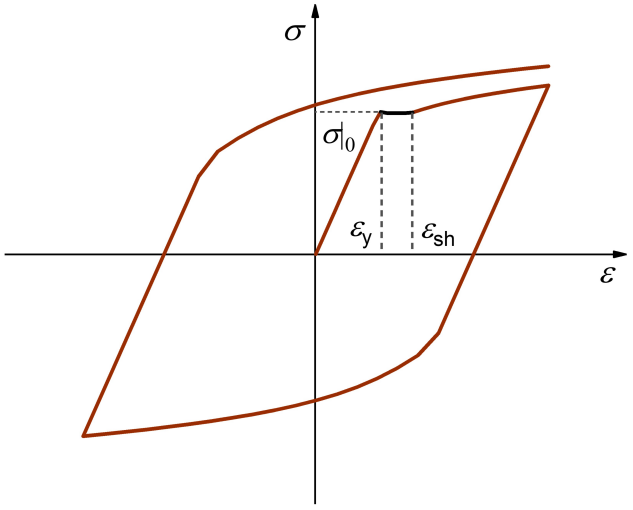

Figure 4. Presence of the yield plateau in the first half cycle idealised as non-hardening region, representation according to [4].

Bild 4. Vorhandensein des Fließplateaus im ersten Halbzyklus idealisiert als nichtverfestigte Region, Darstellung nach [4].

2.2 Nonlinear hardening models

In Abaqus, the cyclic elastic-plastic material behaviour can be described using a combined isotropic-kinematic hardening model proposed by Lemaitre and Chaboche [3]. A detailed overview of the underlying constitutive equations of plasticity theory can be found in the literature [1–6]. For the sake of consistency, the notation used in this paper corresponds to the Abaqus documentation [7]. Hereafter, the von Mises yield criterion is assumed, which can be expressed as a function of the deviatoric stress tensor S, the deviatoric part of the back stress tensor α^{dev} and the current yield stress σ^0:

$$F = \sqrt{\frac{3}{2}(S - \alpha^{dev}) : (S - \alpha^{dev})} - \sigma^0 = 0 \qquad (1)$$

Moreover, the evolution of the plastic deformation under yielding is described using the associated flow rule. Depending on the equivalent (accumulated) plastic strain rate $\dot{\bar{\varepsilon}}^{pl}$, the rate of plastic flow $\dot{\varepsilon}^{pl}$ can be defined as [7]:

$$\dot{\varepsilon}^{pl} = \dot{\bar{\varepsilon}}^{pl} \frac{\partial F}{\partial \sigma}; \quad \dot{\bar{\varepsilon}}^{pl} = \sqrt{\frac{2}{3}\dot{\varepsilon}^{pl} : \dot{\varepsilon}^{pl}} \qquad (2)$$

The Armstrong-Frederick kinematic hardening model is an extension of Prager's linear hardening rule, which includes an additional recall term to introduce nonlinearity [8, 9]. It is given using the expression below [3]:

© 2022 The Authors. Materialwissenschaft und Werkstofftechnik published by Wiley-VCH GmbH

$$\dot{\alpha} = \frac{2}{3} C \dot{\varepsilon}^{\mathrm{pl}} - \gamma \alpha \dot{\bar{\varepsilon}}^{\mathrm{pl}} \tag{3}$$

The coefficients C and γ represent material parameters, where C is the initial kinematic hardening modulus and γ is defined as the rate at which the kinematic hardening modulus decreases with increasing plastic deformation [2, 7]. Under proportional loading, integrating equation (3) leads to the evolution of the back stress α [3]:

$$\alpha = \psi \frac{C}{\gamma} + \left(\alpha_0 - \psi \frac{C}{\gamma} \right) e^{-\psi\gamma(\varepsilon^{\mathrm{pl}} - \varepsilon^{\mathrm{pl},0})} \tag{4}$$

where α_0 and $\varepsilon^{\mathrm{pl},0}$ are the initial values for the back stress and plastic strain at the beginning of the plastic flow. Depending on the direction of plastic flow, $\psi = 1$ for tension and $\psi = -1$ for compression. The stress is given by the yield condition [3]:

$$\sigma = \psi \sigma^0 + \alpha \tag{5}$$

The Armstrong-Frederick kinematic hardening model leads to an unsatisfactory description of the cyclic material behaviour when the considered strain range increases [3, 6]. Due to that, a superposition of several models according to equation (3) was suggested [6, 10–12]:

$$\alpha = \sum_{i=1}^{M} \alpha_i; \; \dot{\alpha}_i = \frac{2}{3} C_i \dot{\varepsilon}^{\mathrm{pl}} - \gamma_i \alpha_i \dot{\bar{\varepsilon}}^{\mathrm{pl}} \tag{6}$$

This results in an improved and more flexible description of the evolution of the back stress α. In analogy to the Armstrong-Frederick evolution model, equation (5) can be expressed as sum of M back stress components resulting in the Chaboche kinematic hardening model [1, 2]:

$$\sigma = \psi \sigma^0 + \alpha = \psi \sigma^0 + \sum_{i=1}^{M} \psi \frac{C_i}{\gamma_i} + \left(\alpha_0^{(i)} - \psi \frac{C_i}{\gamma_i} \right) e^{-\psi\gamma_i(\varepsilon^{\mathrm{pl}} - \varepsilon^{\mathrm{pl},0})} \tag{7}$$

Based on equation (7), the relation between stress and plastic strain can now be determined for a stabilised cycle. If tension ($\psi = 1$) is assumed and the initial values for the back stress α_0 and plastic strain $\varepsilon^{\mathrm{pl},0}$ are applied, we receive the upper branch of the stress-strain hysteresis curve, *Figure 5* [1]:

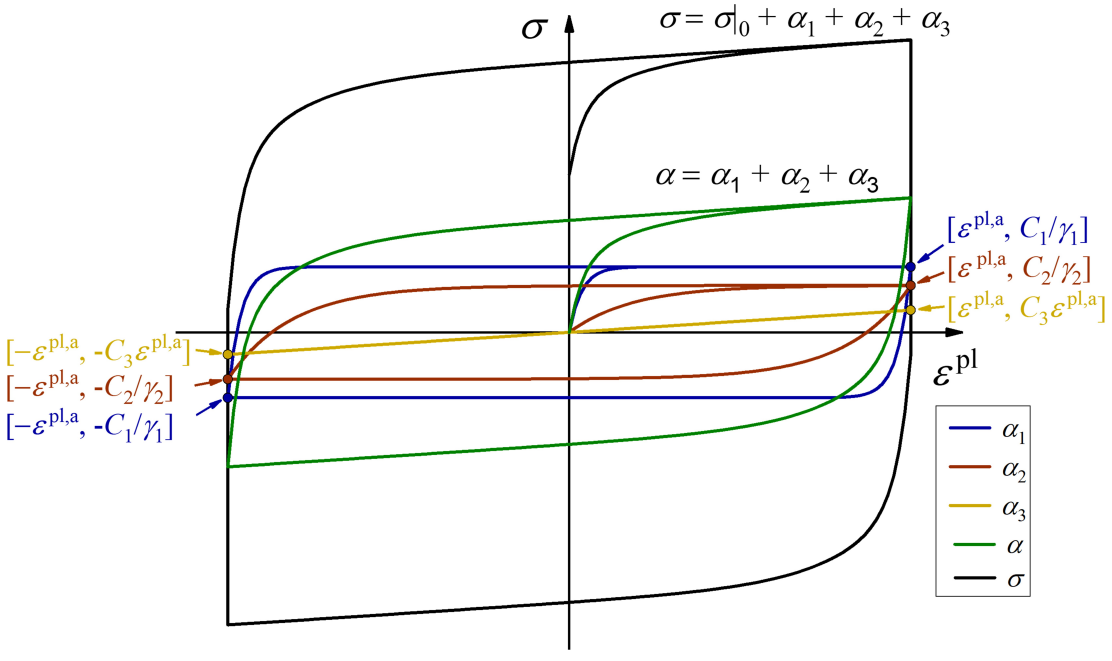

Figure 5. Chaboche kinematic hardening evolution with three back stress components, representation according to [1].

Bild 5. Kinematische Verfestigungsentwicklung nach Chaboche mit drei Rückspannungskomponenten, Darstellung nach [1].

© 2022 The Authors. Materialwissenschaft und Werkstofftechnik published by Wiley-VCH GmbH

$$\sigma = \sigma^0 + \sum_{i=1}^{M} \frac{C_i}{\gamma_i}\left(1 - 2e^{-\gamma_i\left(\varepsilon^{\mathrm{pl}} + \varepsilon^{\mathrm{pl,a}}\right)}\right) \quad (8)$$

The resulting set of parameters (C_i, γ_i) should not be directly interpreted as material properties, but as a decomposition of the simpler Armstrong-Frederick evolution law [6]. The accurate description of the cyclic material behaviour using the Chaboche kinematic hardening model usually requires not more than three back stress components α_i, Figure 5. Considering the ratchetting and mean stress relaxation effect, the evolution of the last back stress component should be defined according to Prager's linear hardening rule ($\gamma_M = 0$) [1, 3]. Hence, equation (8) can be rewritten as:

$$\sigma = \sigma^0 + \sum_{i=1}^{M-1} \frac{C_i}{\gamma_i}\left(1 - 2e^{-\gamma_i\left(\varepsilon^{\mathrm{pl}} - \varepsilon^{\mathrm{pl,a}}\right)}\right) + C_M \varepsilon^{\mathrm{pl}} \quad (9)$$

Isotropic hardening can be described using Voce's exponential law [13]. The evolution of the yield surface size σ^0 is defined as a function of the equivalent plastic strain $\bar{\varepsilon}^{\mathrm{pl}}$ considering the initial yield surface size $\sigma|_0$, the maximum change in the size of the yield surface Q_∞ and the speed of stabilisation b [3, 6, 7]:

$$\sigma^0 = \sigma|_0 + Q_\infty\left(1 - e^{-b\bar{\varepsilon}^{\mathrm{pl}}}\right) \quad (10)$$

Alternatively, the evolution of σ^0 can be expressed by a multilinear relation, where σ_i^0 is the equivalent stress which defines the size of the yield surface depending on $\bar{\varepsilon}^{\mathrm{pl}}$ [4, 7]:

$$\sigma^0 = \sigma|_0 + \left(\sigma_i^0\left(\bar{\varepsilon}^{\mathrm{pl}}\right) - \sigma|_0\right) \quad (11)$$

If isotropic and kinematic hardening evolution equations are both considered simultaneously, we receive the combined isotropic-kinematic hardening model, *Figure 6*. Isotropic hardening covers the uniform expansion of the yield surface in stress space under the development of plastic strain which can be interpreted as the change of the elastic domain [1, 3]. As a result, cyclic softening/hardening is accounted for. Kinematic hardening results in a translation of the yield surface in the direction of the plastic flow which captures the cyclic material behaviour in terms of Bauschinger effect, ratchetting and mean stress relaxation.

3 Experimental cyclic testing

3.1 Material

The material analysed in this study is a fully-processed non-oriented electrical steel sheet with a nominal thickness of 270 µm and the following composition (mass fraction): 3.32 % silicon, 1.10 % aluminium, 0.16 % manganese, 0.01 % carbon,

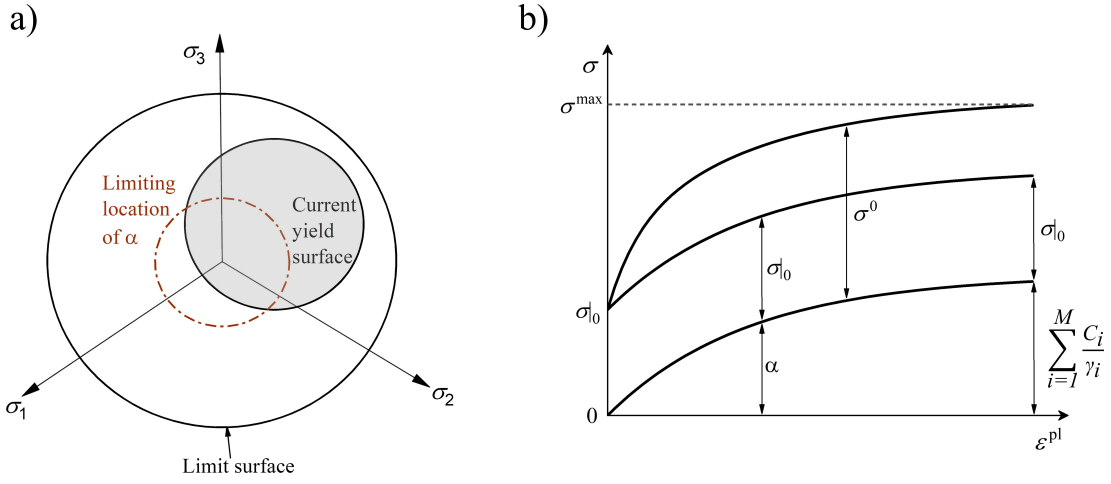

Figure 6. Representation of the combined isotropic-kinematic hardening model, a) in stress-space, b) one-dimensional [7].

Bild 6. Darstellung des kombinierten isotrop-kinematischen Verfestigungsmodells, a) im Spannungsraum, b) eindimensional [7].

© 2022 The Authors. Materialwissenschaft und Werkstofftechnik published by Wiley-VCH GmbH

0.002 % sulfur, 0.010 % phosphorus, balance iron. Therefore, the material exhibits a ferritic microstructure with small non-metallic inclusions. The average grain size is approximately 100 µm, determined by electron backscatter diffraction (EBSD).

Monotonic material properties were determined for ten specimens by quasi-static uniaxial tensile tests at room temperature with a constant strain rate of $2.5 \cdot 10^{-4}\ s^{-1}$, *Table 1*. Due to a slight rolling texture, strength values and Young's modulus in the rolling direction are lower than in other orientations. Hence, in this study, the material is investigated exclusively in rolling direction.

The average Young's modulus and Poisson's ratio in rolling direction is 187 GPa and 0.28, respectively. The material exhibits a small yield plateau with an average yield strength of 447 MPa. Under quasi-static loading, the material shows a limited amount of hardening, resulting in a comparatively flat stress-strain curve with an ultimate tensile strength of 540 MPa and an elongation at break of 15 %, *Figure 7*.

Table 1. Monotonic material properties of the studied electrical steel sheets in rolling direction.

Tabelle 1. Monotone Werkstoffeigenschaften der untersuchten Elektrobleche in Walzrichtung.

Young's modulus E [GPa]	Poisson's ratio ν [–]	Yield strength $\sigma\|_0$ [MPa]	Ultimate tensile strength R_m [MPa]	Elongation at break A_t [%]
187	0.28	447	540	15.3

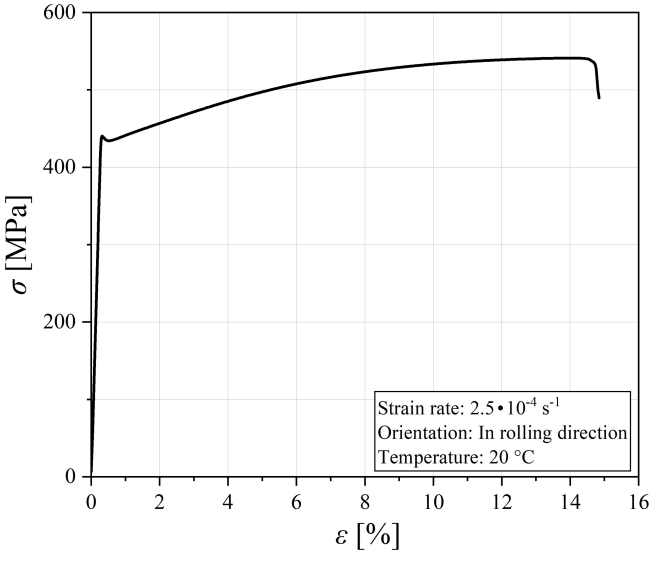

Figure 7. Monotonic tensile stress-strain curve of the studied electrical steel sheets.

Bild 7. Monotone Spannungs-Dehnungs-Kurve der untersuchten Elektrobleche unter Zugbeanspruchung.

3.2 Test setup

Experimental results are obtained from symmetric strain-controlled cyclic tests. For thin electrical steel sheets, most authors use stress-controlled cyclic tests without compression forces, among other reasons, to avoid buckling of the specimens. However, strain-controlled tests are preferably used to characterise the cyclic stress-strain behaviour and therefore, to perform the calibration of the combined isotropic-kinematic hardening material model. Consequently, in this study, all cyclic tests are performed with symmetric strain amplitudes at room temperature with a constant strain rate of $5 \cdot 10^{-3}\ s^{-1}$. Cyclic loading is applied by means of an electric dynamic test machine Electro-Puls E10000 from INSTRON and an extensometer EXA 10-0,5 from SANDNER-Messtechnik GmbH is used. The calibration and alignment of the testing machine are in accordance with DIN EN ISO 7500-1 and ISO 23788, respectively.

Due to the low thickness of the electrical steel sheets, an anti-buckling device is necessary to avoid buckling of the specimen and for proper extensometer mounting, *Figure 8*a. Tests are performed with five different strain amplitudes ε_a between 0.2 % and 0.6 %. Despite using an anti-buckling device, the testing of high strain amplitudes ($\varepsilon_a > 0.6\ \%$) is only possible to a limited extent, since the results are increasingly influenced by occurring waviness the higher the compressive forces get. Therefore, only tests until a strain amplitude of $\varepsilon_a = 0.6\ \%$ are considered in the present study.

The two halves of the anti-buckling device are fastened by four screws to the sample, Figure 8b. Two vertical guide rails are used to restrict unintended movement of the anti-buckling device during the cyclic test. A diamond-like carbon (DLC) coating reduces friction at the sliding contact between anti-buckling-device and specimen. Furthermore, polytetrafluoroethylene-foil is used at the sliding contact between vertical guide rails and

© 2022 The Authors. Materialwissenschaft und Werkstofftechnik published by Wiley-VCH GmbH

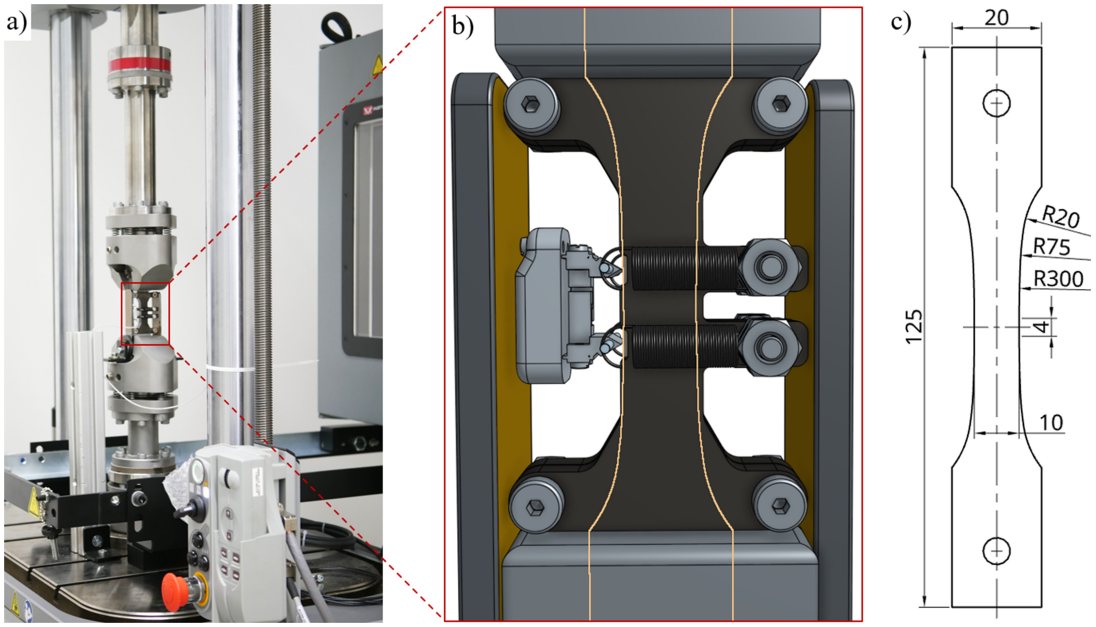

Figure 8. Experimental setup, a) test machine setup, b) detailed view of the anti-buckling device with vertical guide rails, extensometer, tension springs and specimen, the latter highlighted by a yellow line, c) specimen geometry.

Bild 8. Versuchsaufbau, a) Versuchsmaschinenaufbau, b) Detailansicht der Knickstütze mit vertikalen Führungsschienen, Extensometer, Zugfedern und Probe, letztere durch eine gelbe Linie hervorgehoben, c) Probengeometrie.

anti-buckling device. A small gap must remain between anti-buckling device and clamping jaws to avoid buckling and allow unrestricted extension and compression of the specimen. Due to the anti-buckling device, the positioning of the extensometer is limited to the small edges of the samples. By using tension springs for proper mounting, slippage can be prevented. However, the small contact area between the cutting edge of the extensometer and the specimen edge can lead to high local surface pressures. It therefore has to be ensured that no crack initiation starting from this contact area is observed.

Cyclic tests are performed with smooth specimens ($R_z < 1.0\,\mu m$), which are processed from sheet material by high precision electrical discharge machining (EDM). In this study, flat specimens with 4 mm gauge length and 10 mm width are used, Figure 8c. The transition area is designed with three matching radii to achieve a homogeneous stress state with a minimised notch factor.

3.3 Results

The experimental results include representative stress-strain hysteresis curves at 90 % of fatigue life, *Figure 9*. Usually, representative hysteresis

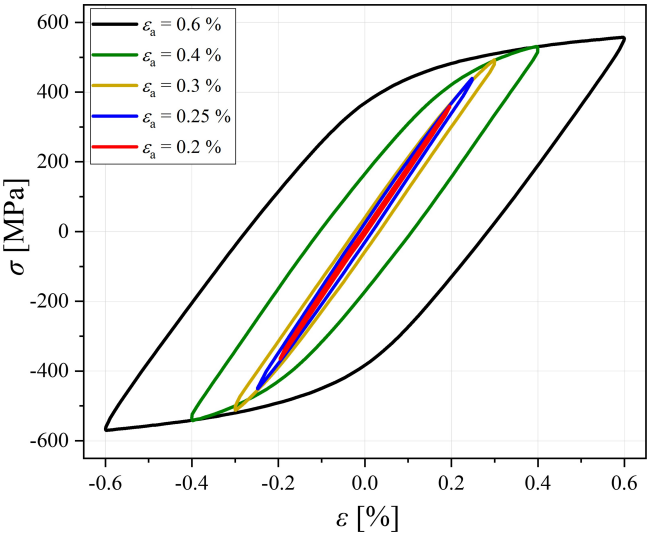

Figure 9. Experimental stress-strain hysteresis curves at 90 % of fatigue life.

Bild 9. Experimentelle Spannungs-Dehnungs-Hysteresekurven bei 90 % der Ermüdungslebensdauer.

© 2022 The Authors. Materialwissenschaft und Werkstofftechnik published by Wiley-VCH GmbH

curves are defined at 50 % of fatigue life, which is based on the assumption that the material behaviour has stabilised at half of the number of cycles to failure. However, in the case of the studied electrical steel, no stabilised condition is reached during the cyclic test. Instead, the material exhibits cyclic hardening until crack initiation, *Figure 10*. Therefore, to describe the material behaviour appropriately, hysteresis curves are selected at 90 % of fatigue life. It is ensured that the chosen stress-strain hysteresis curves do not yet have a crack, as its presence influences the hysteresis shape.

The extend of cyclic softening/hardening is revealed by the cyclic accommodation curves considering the five different strain amplitudes, Figure 10. In general, a division into three material responses can be made depending on the strain hardening behaviour:

- For tests performed at high strain amplitudes ($\varepsilon_a = 0.4$ %, and $\varepsilon_a = 0.6$ %), the material exhibits substantial cyclic hardening without stabilisation until fracture. The stress amplitude rises to values slightly higher than the ultimate tensile strength measured in the tensile tests.
- For tests performed at strain amplitudes $\varepsilon_a = 0.25$ % and $\varepsilon_a = 0.3$ % a slight softening behaviour is observed at the beginning before rapid cyclic hardening occurs.
- Regarding the lowest strain amplitude $\varepsilon_a = 0.2$ %, only slight changes of the stress response are observed. No plastic deformation takes place, which is why these tests will not be considered further on.

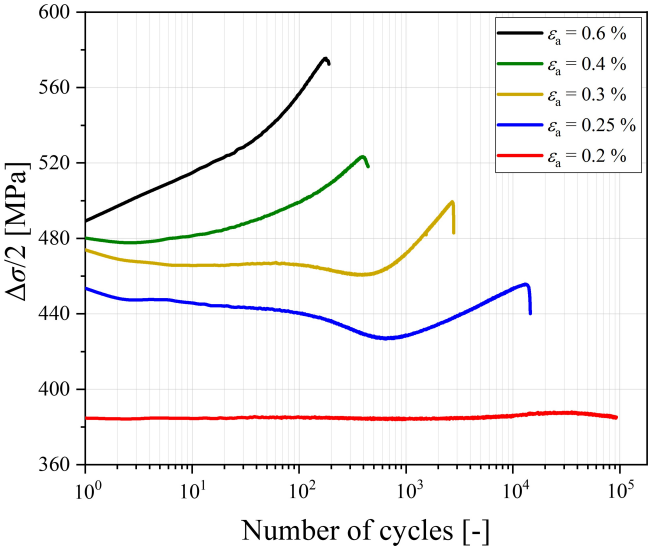

Figure 10. Cyclic deformation behaviour of the studied electrical steel sheets showing continuous cyclic hardening without saturation until failure.

Bild 10. Wechselverformungsverhalten der untersuchten Elektrobleche zeigt kontinuierliche zyklische Verfestigung ohne Stabilisierung bis zum Versagen.

4 Determination of material parameters: material model calibration

4.1 Fundamentals

On the one hand, the material model calibration in Abaqus includes the definition of the elastic properties described by Young's modulus E and Poisson's ratio ν according to the results of the monotonic uniaxial tensile tests, Table 1. On the other hand, the combined isotropic-kinematic hardening parameters describing the plastic material behaviour must be calibrated based on the conducted symmetric strain-controlled cyclic tests.

The kinematic hardening parameters can be determined by the stabilised stress-strain hysteresis curve, *Figure 11*a [1, 7]. This usually provides accurate results for the considered strain range $\Delta\varepsilon$, as long as the hysteresis curves are not expected to significantly differ in shape for varying strains. The isotropic hardening parameters are determined using the sequence of the stress-strain hysteresis curves of a complete cyclic test, Figure 11b.

It has to be considered that the experimental test data is described in terms of nominal stress σ_{nom} and engineering strain ε_{nom}. Since the material model calibration in Abaqus requires the true stress and logarithmic strain as input data, the following relations are used to convert into the respective quantities:

$$\sigma = \sigma_{nom}(1 + \varepsilon_{nom}) \tag{12}$$

$$\varepsilon = \ln(1 + \varepsilon_{nom}) \tag{13}$$

4.2 Kinematic hardening component

The parameter set of the kinematic hardening component (C_i, γ_i) can be obtained by fitting equa-

© 2022 The Authors. Materialwissenschaft und Werkstofftechnik published by Wiley-VCH GmbH

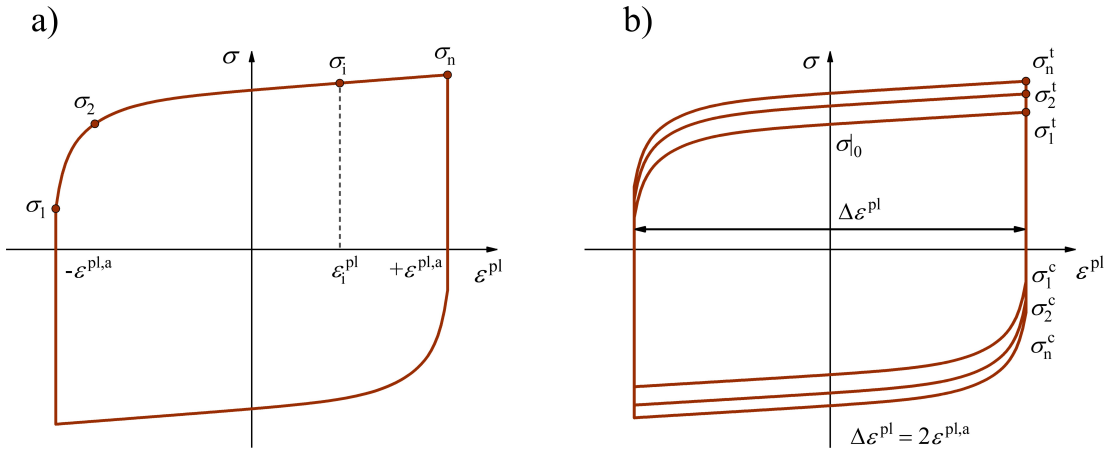

Figure 11. Quantities of the stress-strain hysteresis curves for the determination of a) kinematic hardening, b) isotropic hardening [7].

Bild 11. Größen der Spannungs-Dehnungs-Hysterese-Kurven zur Bestimmung von a) kinematischer Verfestigung, b) isotroper Verfestigung [7].

tion (9) to data pairs (σ_i,ε_i^{pl}) of the stabilised stress-strain hysteresis curve [1]. The calibration can be performed using the Abaqus internal fitting routine as well as a nonlinear least-squares regression analysis. The stabilised stress-strain hysteresis curve generally shows an initial steep slope followed by a curved section leading to a flatter region [14]. The data points of the steep sloped region have a more significant influence on the residuals compared to the flatter region. As a result, less weighting is given to the flatter region during the curve fitting process. At the same time, more weighting is given to parts of the curve where data points are more concentrated. Since Abaqus' internal fitting routine does not provide sufficient options to monitor the quality of the fit, the least-squares regression should be performed in an external program. In this paper, the curve fitting toolbox of Matlab is used.

Stabilised stress-strain hysteresis curves at 90 % of fatigue life are available for different strain amplitudes, Figure 9. In order to determine representative parameters, the stabilised hysteresis with the largest strain amplitude ($\varepsilon_a = 0.6$ %) should be considered. Thus, it can be ensured that the parameters are best suitable for a preferably broad strain range $\Delta\varepsilon$. The start and end values ε_1^{pl}, ε_n^{pl} of the prepared data pairs (σ_i,ε_i^{pl}) correspond to the plastic strain amplitude $\pm\varepsilon^{pl,a}$, Figure 11a. Plastic strain values ε_i^{pl} are calculated by subtracting the elastic from the total strain ε_i using the Young's modulus of the stabilised cycle:

$$\varepsilon_i^{pl} = \varepsilon_i - \frac{\sigma_i}{E} \tag{14}$$

The least-squares regression is performed for two and three back stress components α_i, respectively. It can be recognised that the quality of the fit is considerably improved if three back stress components are used, *Figure 12*. The root mean

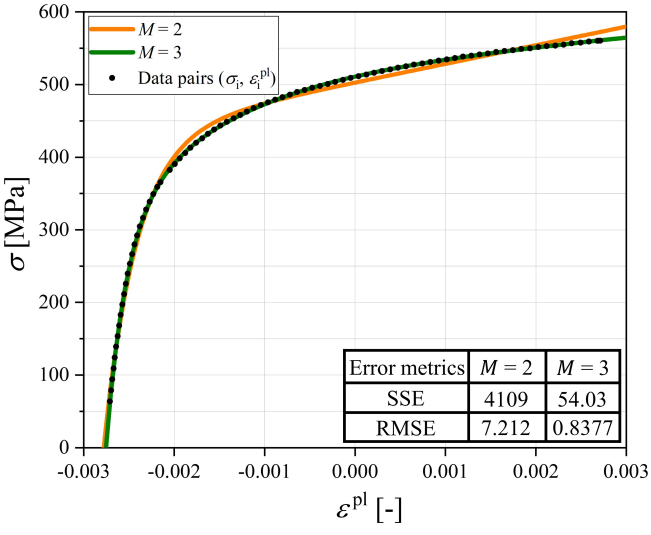

Figure 12. Results of the least-squares regression analysis for the determination of the kinematic hardening component considering two and three back stress components.

Bild 12. Ergebnisse der Kleinste-Quadrate-Regressionsanalyse zur Bestimmung der kinematischen Verfestigungskomponente unter Berücksichtigung von zwei und drei Rückspannungskomponenten.

© 2022 The Authors. Materialwissenschaft und Werkstofftechnik published by Wiley-VCH GmbH

squared error (RMSE) is reduced from a value of 7.2 to 0.84 indicating a reliable fitting result. Both the data points of the steep sloped as well as the flatter region of the curve are accurately captured. The addition of further back stress components is not useful, since only minor adjustments can be expected. With the resulting parameter set, the evolution of kinematic hardening is defined, *Table 2*. For its graphical representation, the respective back stress components are plotted according to equation (4) under consideration of zero initial plastic strain and back stress, *Figure 13*.

4.3 Isotropic hardening component

The isotropic hardening component is determined by calculating the equivalent stress σ^0, which defines the size of the yield surface (elastic range) as a function of the equivalent plastic strain $\bar{\varepsilon}^{pl}$ [7]. Data pairs (σ_i^0, $\bar{\varepsilon}_i^{pl}$) should be provided for a range of equivalent plastic strain which is of interest for the simulation. This usually refers to the condition until stabilisation of the hysteresis curves occurs. As mentioned before, electrical steel continuously exhibits cyclic hardening. The equivalent stress σ^0 defining the size of the yield surface should therefore be calibrated until 90 % of fatigue life. At zero equivalent plastic strain, the initial yield surface size $\sigma|_0$ is defined as the material's yield strength. With the peak tensile stress σ_i^t and the maximum compression stress σ_i^c in the elastic range, the yield surface size of the i^{th} cycle can be calculated, Figure 11b:

$$\sigma_i^0 = \frac{\sigma_i^t - \sigma_i^c}{2} \tag{15}$$

The corresponding equivalent plastic strain can be expressed as a function of the cycle number and the plastic strain range $\Delta\varepsilon^{pl}$ which can be approximately calculated with the Young's modulus E and the peak tensile stress of the first cycle σ_1^t. Using the following relations, both quantities can be assessed [7]:

$$\Delta\varepsilon^{pl} \approx \Delta\varepsilon - \frac{2\sigma_1^t}{E} \tag{16}$$

$$\bar{\varepsilon}_i^{pl} = \frac{1}{2}(4i-3)\Delta\varepsilon^{pl} \tag{17}$$

The stress-strain hysteresis curves usually show imperfections [15]. This leads to a deviation from the shape of an idealised hysteresis curve, Figure 11. The imperfections include, for example, strain data slightly exceeding the adjusted strain range and no sharp corners of the hysteresis curve. Moreover, the symmetric strain-controlled cyclic tests of electrical steel sheet specimens are limited to a relatively small strain range due to buckling problems. Although the individual deviations are small, the combined effect of the errors results in uncertainties [15]. Hence, the identification of the actual elastic range becomes a quite difficult task, *Figure 14*.

To allow for an appropriate estimation nevertheless, it is proposed to apply a vertical line in the middle area of the rounded corner of the hysteresis

Table 2. Resulting kinematic hardening parameters of the three back stress components.

Tabelle 2. Resultierende kinematische Verfestigungsparameter der drei Rückspannungskomponenten.

C_1 [MPa]	γ_1 –	C_2 [MPa]	γ_2 –	C_3 [MPa]	γ_3 –
568467	4566	79017	817.9	11500	0

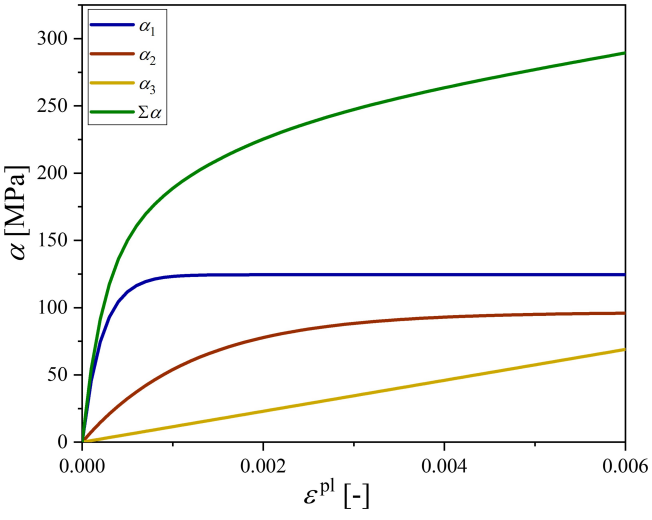

Figure 13. Evolution of the calculated back stress components considering zero initial back stress and plastic strain.

Bild 13. Entwicklung der berechneten Rückspannungskomponenten unter Berücksichtigung von Null-Anfangsrückspannung und plastischer Dehnung.

© 2022 The Authors. Materialwissenschaft und Werkstofftechnik published by Wiley-VCH GmbH

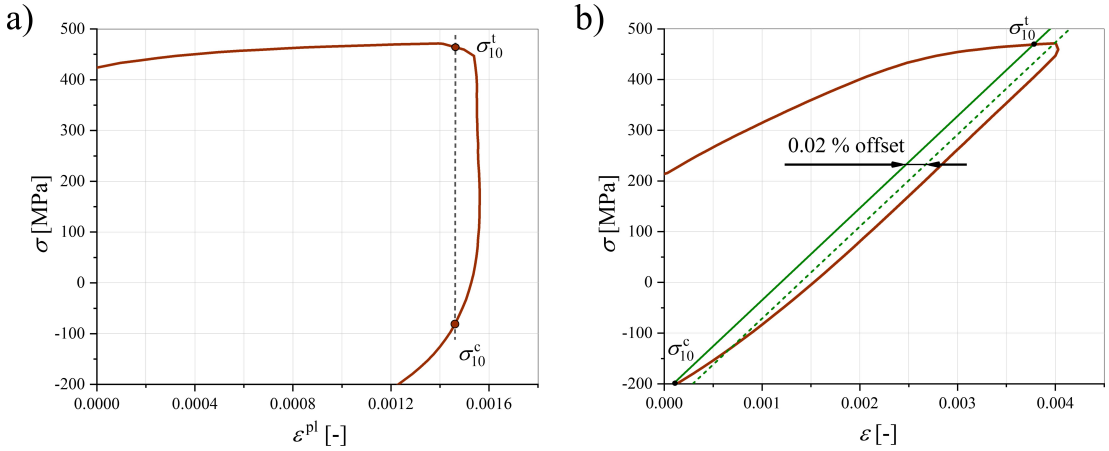

Figure 14. Identification of the elastic range of a stress-strain hysteresis curve deviating from the idealised shape by a) vertical line, b) 0.02 % offset method according to [15].

Bild 14. Identifizierung des elastischen Bereichs einer Spannungs-Dehnungs-Hysterese-Kurve abweichend von der idealisierten Form durch a) vertikale Linie, b) 0,02 % Offset-Methode nach [15].

curve, Figure 14a. The resulting intersections can be considered as the peak tensile stress and compressive stress in the elastic range. Alternatively, it is possible to determine the elastic range by applying a straight line with the slope of the Young's modulus of the respective cycle, Figure 14b. Starting from the upper right corner, the end of the elastic range (maximum compression stress) is reached, when the hysteresis curve begins to separate to a certain degree from the straight line. With respect to the described imperfections of the hysteresis curves, it is suggested to apply the straight line not at the point of nominal strain amplitude, but with a 0.02 % offset in the negative strain direction [15]. Both methods cannot avoid the described uncertainties, especially for small strain amplitudes below 0.3 %, since the separation of elastic and plastic portions becomes increasingly difficult. However, the approach including the application of a vertical line is expected to represent the better estimation of the elastic range for electrical steel, Figure 14a.

It is important to note that the amount of isotropic hardening depends on the magnitude of the equivalent (accumulated) plastic deformation [1, 7]. As a result, the data pairs $(\sigma_i^0, \bar{\varepsilon}_i^{\mathrm{pl}})$ of the isotropic hardening component have to be individually determined for the different considered strain amplitudes, *Figure 15*. It shows that, regardless of the strain amplitude, the yield surface size decreases in the first half cycle due to the presence of the yield

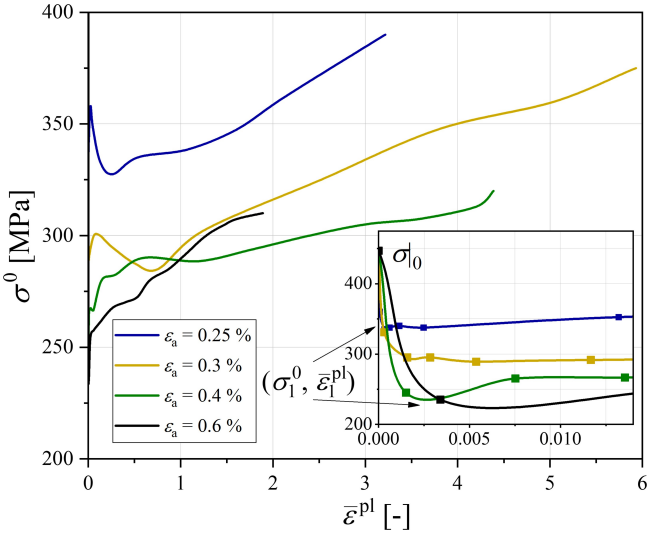

Figure 15. Evolution of isotropic hardening represented by calculated data pairs $(\sigma_i^0, \bar{\varepsilon}_i^{\mathrm{pl}})$.

Bild 15. Entwicklung der isotropen Verfestigung dargestellt durch berechnete Datenpaare $(\sigma_i^0, \bar{\varepsilon}_i^{pl})$.

plateau. This corresponds to cyclic softening from the initial yield surface size $\sigma|_0$. After the first load reversal, the yield plateau disappears and the yield surface size increases over the number of load cycles as cyclic hardening occurs, Figure 10.

Thus, the evolution law of the yield surface size has to account for the monotonic behaviour in the first half cycle (initial cyclic softening) and subsequently for the actual cyclic behaviour by using different slopes. Describing the data pairs $(\sigma_i^0, \bar{\varepsilon}_i^{\mathrm{pl}})$

© 2022 The Authors. Materialwissenschaft und Werkstofftechnik published by Wiley-VCH GmbH

with Voce's law according to equation (10), two sets of parameters ($\sigma|_0$, Q_∞, b) have to be provided. The rapid decrease of the yield surface size has to be expressed with a negative maximum change in the size of the yield surface Q_∞ which equals the difference between σ_1^0 and $\sigma|_0$. The speed of stabilisation b can then be determined by least-squares regression analysis. In contrast, the increase of the yield surface size is defined by a positive value of Q_∞. The required parameters are obtained by least-squares regression using the data between σ_1^0 and σ_n^0. The determination of both the monotonic and cyclic parameter set is performed for the strain amplitude $\varepsilon_a = 0.4\ \%$, *Table 3*. On this basis, the corresponding evolution of the yield surface size can be plotted, *Figure 16*.

Table 3. Monotonic and cyclic parameter set of the isotropic hardening evolution for $\varepsilon_a = 0.4\ \%$ according to Voce's law.

Tabelle 3. Monotoner und zyklischer Parametersatz der isotropen Verfestigungsentwicklung für $\varepsilon_a = 0{,}4\ \%$ nach dem Gesetz von Voce.

Parameter set	Monotonic	Cyclic
$\sigma\|_0$ [MPa]	447	256
Q_∞ [MPa]	−202	49.56
b [−]	6613	0.6645

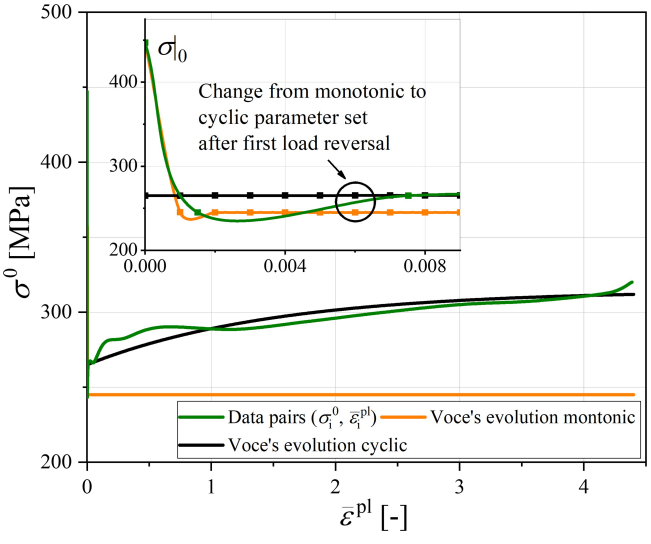

Figure 16. Evolution of isotropic hardening for $\varepsilon_a = 0.4\ \%$ represented by Voce's law.

Bild 16. Entwicklung der isotropen Verfestigung für $\varepsilon_a = 0{,}4\ \%$ dargestellt durch das Voce'sche Gesetz.

The description of the isotropic hardening component with Voce's law results in certain difficulties. The simultaneous implementation of initial cyclic softening and subsequent cyclic hardening requires changing the monotonic to the cyclic parameter set after the first load reversal. This change can lead to an unintended discontinuity in the stress-strain relation and consequently to stability problems in the material model definition in Abaqus. Moreover, the exponential decline of the isotropic hardening component during the initial cyclic softening causes convergence issues. To prevent such problems, the isotropic hardening component should be defined using the multilinear approach according to equation (11). It enables different slopes in the evolution of the isotropic hardening, which makes it more flexible than Voce's exponential law. With the multilinear approach, the calculated data pairs (σ_i^0, $\bar{\varepsilon}_i^{pl}$) are connected assuming a linear relation between them.

The rapid decrease of the yield surface size in the first half cycle is only described by the first two data points ($\sigma|_0$, 0) and (σ_1^0, $\bar{\varepsilon}_1^{pl}$). To allow for a more accurate representation of the yield plateau, an alternative calibration of the isotropic hardening component is suggested. If the stress-strain relation of the first half cycle $\sigma(\bar{\varepsilon}^{pl}) = \sigma(\varepsilon^{pl})$ and the evolution of the kinematic hardening component α are known, equation (7) can be solved for the corresponding evolution of isotropic hardening σ^0:

$$\sigma^0(\bar{\varepsilon}^{pl}) = \sigma(\bar{\varepsilon}^{pl}) - \alpha \tag{18}$$

For this purpose, the monotonic stress-strain relation is experimentally determined under the same test conditions as for the cyclic tests, *Figure 17*a. It has to be considered that the subsequent implementation in Abaqus requires a monotonously increasing stress-strain relation in the material model definition in order to prevent convergence issues. Since the experimental data shows the presence of an upper and lower yield point, it should be smoothed for further calculations. In accordance with equation (5), the data pairs can be described by means of a least-squares regression analysis using Prager's linear hardening rule, Figure 17b.

The resulting evolution of the isotropic hardening component σ^0 is plotted for the first half cycle, *Figure 18*. In addition, the evolution of kinematic hardening α is displayed. It shows that the sum of

© 2022 The Authors. Materialwissenschaft und Werkstofftechnik published by Wiley-VCH GmbH

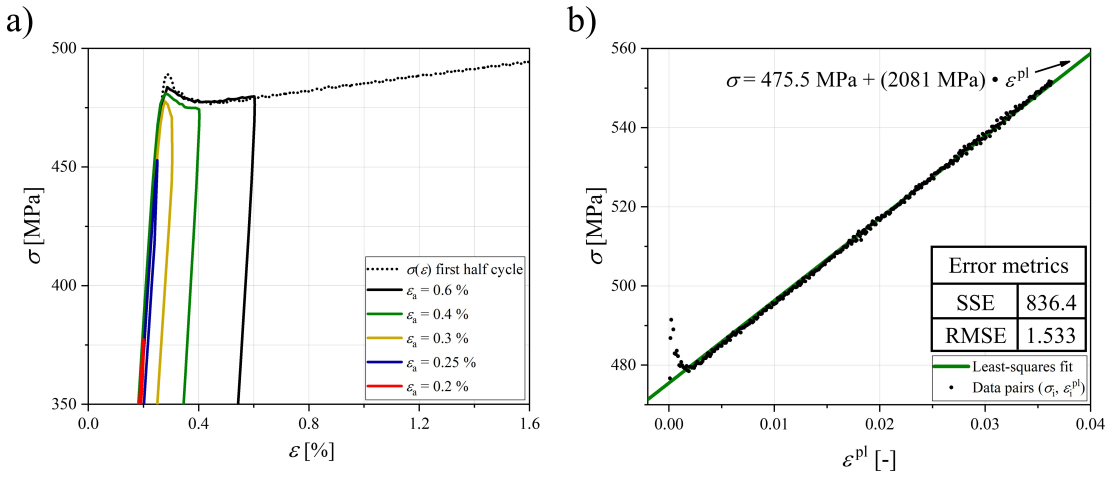

Figure 17. Monotonic stress-strain relation of the first half cycle, a) experiment, b) described by Prager's linear hardening rule.

Bild 17. Monotone Spannungs-Dehnungs-Beziehung des ersten Halbzyklus, a) Versuch, b) beschrieben durch die lineare Verfestigungsregel von Prager.

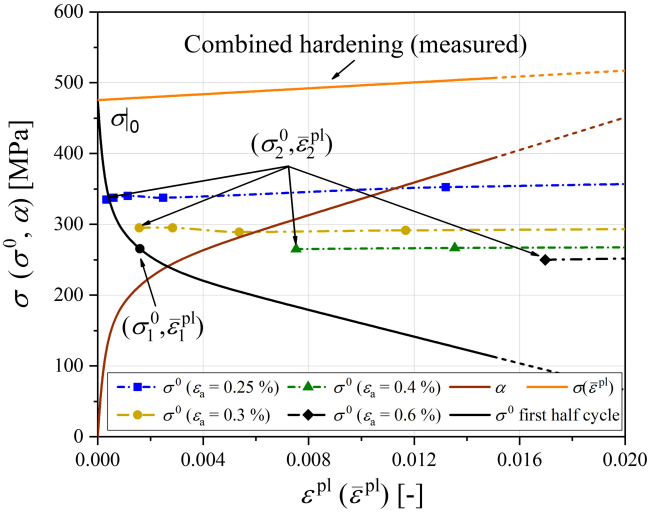

Figure 18. Resulting evolution of isotropic, kinematic and combined hardening for the first half cycle including indicated onset of cyclic hardening.

Bild 18. Resultierende Entwicklung der isotropen, kinematischen und kombinierten Verfestigung für den ersten Halbzyklus einschließlich des angedeuteten Beginns der zyklischen Verfestigung.

isotropic and kinematic hardening equals the desired stress-strain-relation of the first half cycle. According to that, the calculation using equation (18) can be interpreted as a decomposition of combined hardening $\sigma(\bar{\varepsilon}^{\mathrm{pl}})$ to determine the decrease of the yield surface size until the first load reversal. To not only represent the monotonic behaviour in the first half cycle, the evolution of the yield surface size has to be complemented by the subsequent cyclic hardening. Therefore, the calculated data pairs $(\sigma_i^0,\ \bar{\varepsilon}_i^{\mathrm{pl}})$ including values between the second $(\sigma_2^0,\ \bar{\varepsilon}_2^{\mathrm{pl}})$ and the last cycle $(\sigma_{\mathrm{n}}^0,\ \bar{\varepsilon}_{\mathrm{n}}^{\mathrm{pl}})$ have to be considered as well. This is indicated by dashed lines for the different strain amplitudes, Figure 18. The equivalent plastic strain reached at the point of the first load reversal corresponds to the data pair of the first cycle $(\sigma_1^0,\ \bar{\varepsilon}_1^{\mathrm{pl}})$. It can be interpreted as the end of the initial cyclic softening and the onset of the cyclic hardening. As before, the initial size of the yield surface $\sigma|_0$ is defined at zero equivalent plastic strain.

5 Finite-element model implementation in Abaqus

5.1 Simulation setup

After the calibration of kinematic and isotropic hardening parameters, the material behaviour of electrical steel can be simulated in Abaqus. The specimen geometry used in this study is analysed in a two-dimensional static simulation using general-purpose shell elements of type S4R (four-node shell, reduced integration), *Figure 19*. According to mesh sensitivity studies, an element size of 1 mm is chosen for the upper and lower end of the specimen. In the gauge and transition area, the mesh density is refined using an element size of 0.7 mm.

© 2022 The Authors. Materialwissenschaft und Werkstofftechnik published by Wiley-VCH GmbH

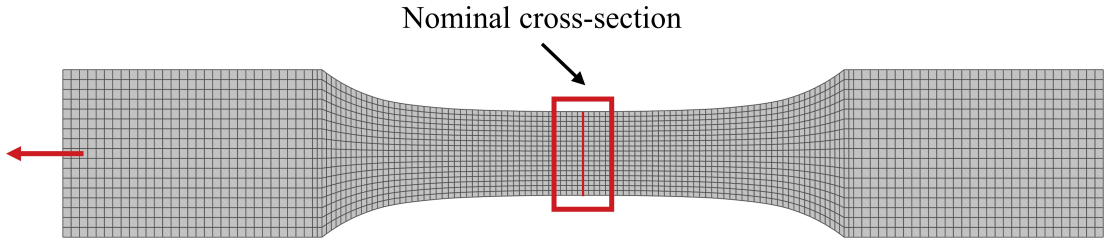

Figure 19. Two-dimensional model of the electrical steel sheet specimen for the numerical simulation of cyclic loading.
Bild 19. Zweidimensionales Modell der Elektroblechprobe zur numerischen Simulation der zyklischen Beanspruchung.

The boundary conditions correspond to the setup of the experimental cyclic tests. The uniaxial cyclic load is applied at the upper end of the specimen, whereas the lower end remains fixed. For stress-controlled loading, the magnitude of the effective force is defined by the nominal cross-section of the specimen. To enable a strain-controlled simulation, the applied displacement amplitude has to be updated depending on the resulting amount of strain [16]. In this study, a Python script is implemented to iteratively calculate the displacement amplitude corresponding to a constant strain amplitude in the specimen's nominal cross-section.

In the context of the material model definition, the kinematic hardening component is directly defined by the presented parameters, Table 2. The isotropic hardening component on the other side is defined in two steps. In the first step, it is only defined for the monotonic behaviour in the first half cycle according to equation (18). The relation $\sigma^0\left(\bar{\varepsilon}^{\mathrm{pl}}\right)$ is provided in tabular form including data pairs (σ^0, $\bar{\varepsilon}^{\mathrm{pl}}$) from 0 to 1.5 % equivalent plastic strain, Figure 18. As mentioned before, Abaqus assumes a linear relation between the individual data pairs. For an accurate description of the isotropic hardening $\sigma^0\left(\bar{\varepsilon}^{\mathrm{pl}}\right)$, a small equivalent plastic strain increment (e. g., $\bar{\varepsilon}^{\mathrm{pl}} = 1 \cdot 10^{-5}$) should therefore be considered.

On this basis, the simulation of the monotonic behaviour is performed by calculating the equivalent plastic strain $\bar{\varepsilon}_1^{\mathrm{pl}}$ reached at the point of the first load reversal. With this information, the isotropic hardening component can be subsequently updated for the simulation of the complete load sequence. The data pair (σ^0, $\bar{\varepsilon}^{\mathrm{pl}}$), which corresponds to the equivalent plastic strain $\bar{\varepsilon}_1^{\mathrm{pl}}$, marks the end of the previously defined monotonic behaviour. Then, the cyclic behaviour is defined by the calculated data pairs between the second (σ_2^0, $\bar{\varepsilon}_2^{\mathrm{pl}}$) and the last cycle ($\sigma_{\mathrm{n}}^0$, $\bar{\varepsilon}_{\mathrm{n}}^{\mathrm{pl}}$) selected for the respective strain range, Figure 18.

If the strain range expected in the simulation differs from those which have been considered for the calibration of the isotropic hardening component, no calculated data pairs are available. In this case, it is possible to estimate the evolution of isotropic hardening (σ_2^0, $\bar{\varepsilon}_2^{\mathrm{pl}}$) to ($\sigma_{\mathrm{n}}^0$, $\bar{\varepsilon}_{\mathrm{n}}^{\mathrm{pl}}$) by linear interpolation for strain ranges that lie between the known data pairs. Moreover, the evolution of isotropic hardening can be extrapolated for expected strain ranges exceeding the calibrated data. However, the extrapolation should be treated carefully, since the evolution of the yield surface size cannot be generalised for significantly smaller or larger strain ranges. Instead of extrapolating data pairs, the isotropic hardening component can be assumed to be constant after the equivalent plastic strain $\bar{\varepsilon}_1^{\mathrm{pl}}$ is reached. As a result, the initial cyclic softening due to the yield plateau is accounted for, while subsequent cyclic softening/hardening is neglected.

5.2 Results and validation with experimental cyclic tests

The comparison between simulation and experimental data is shown for a symmetric strain-controlled cyclic loading including the strain amplitudes considered in the material model calibration, *Figure 20*. For each strain amplitude, the first three cycles are represented. It can be seen that the predicted material behaviour is basically in good agreement with the experimental cyclic tests. The yield plateau in the first half cycle as well as the onset of the cyclic behaviour are properly described. Considering the strain amplitudes $\varepsilon_{\mathrm{a}} = 0.3\,\%$, $\varepsilon_{\mathrm{a}} = 0.4\,\%$ and $\varepsilon_{\mathrm{a}} = 0.6\,\%$, the shape and width of the stress-strain hysteresis curves are

© 2022 The Authors. Materialwissenschaft und Werkstofftechnik published by Wiley-VCH GmbH

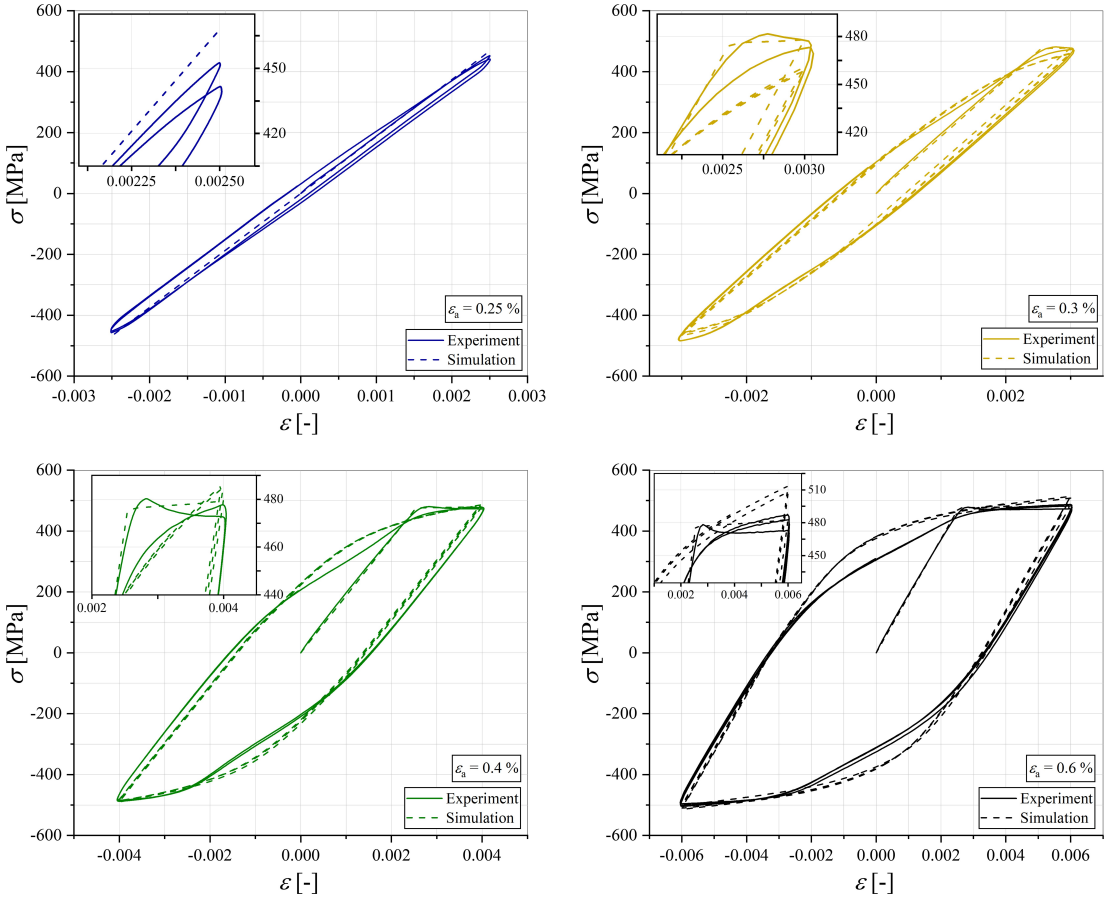

Figure 20. Comparison of simulation and experimental data for symmetric strain-controlled cyclic loading with respect to the first three cycles.

Bild 20. Vergleich von Simulation und Versuchsdaten für symmetrische dehnungskontrollierte zyklische Belastung in Bezug auf die ersten drei Zyklen.

accurately predicted. Minor differences can be explained by the influence of the anti-buckling device on the load cycles. Especially when the loading direction is reversed, friction between specimen and anti-buckling device has to be overcome which affects the stress-strain relation in an irregular way.

Moreover, the experimentally determined hysteresis curves exhibit rounded corners as already discussed in the context of imperfect cyclic test data. This behaviour seems to be related to time-dependent plastic deformation caused by stress relaxation under strain-controlled loading [17]. As a result, the plastic strain continues to increase even though the maximum stress is reached. For the strain amplitude $\varepsilon_a = 0.25$ %, it becomes apparent that the experimental data shows a small amount of plastic deformation, whereas the material's yield strength is not exceeded, Figure 17. The simulation on the other side predicts linear elastic material behaviour. An explanation for this deviation could be the previously described time-dependent plastic deformation which has a more significant influence on small strain ranges and cannot be accounted for in the material model.

The results for an unsymmetric stress-controlled cyclic loading ($\sigma_{max} = 500$ MPa, $R_\sigma = 0.1$) are considered including the first ten load cycles, *Figure 21*. In contrast to a strain-controlled loading condition, the strain range is not constant. Apart from this, the strain range reached in the first half cycle clearly exceeds the calibrated data of the isotropic hardening component ($\Delta\varepsilon > 0.6$ %). Consequently, the evolution of the yield surface size can only be estimated, as mentioned before. In the present case, the isotropic hardening component is assumed to be constant after the equivalent plastic strain $\bar{\varepsilon}_1^{pl}$ is reached.

© 2022 The Authors. Materialwissenschaft und Werkstofftechnik published by Wiley-VCH GmbH

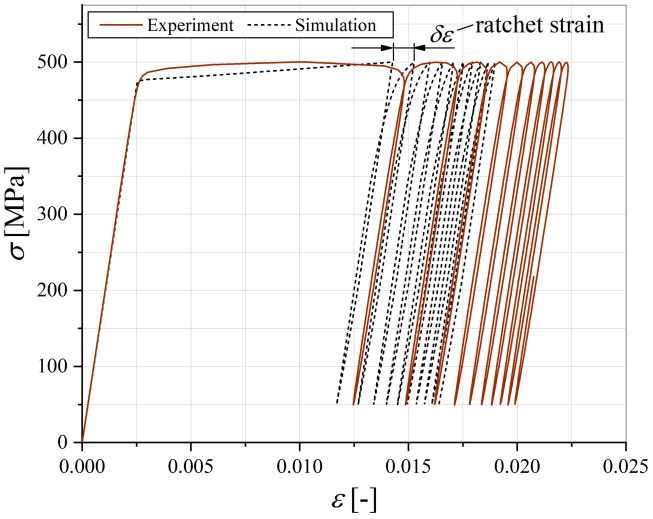

Figure 21. Comparison of simulation and experimental data for unsymmetric stress-controlled cyclic loading with respect to the first ten cycles.

Bild 21. Vergleich von Simulation und Versuchsdaten für unsymmetrische belastungskontrollierte zyklische Belastung in Bezug auf die ersten zehn Zyklen.

The comparison with experimental data shows that the material behaviour in the first half cycle is correctly represented, while the ratchet strain is underestimated. This may be explained by the assumed evolution of the yield surface size. Another possible reason is that the experimentally determined hysteresis curves exhibit distinct rounded corners which again indicates the presence of time-dependent plastic deformation. More precisely, this is associated with a creep deformation process occurring under stress-control [17]. An explicit separation in time-dependent and -independent plastic deformation proves to be difficult. However, the experimental data shows that the location of the maximum stress lies more or less in the middle of the rounded corners of the hysteresis curves. If the plastic strain is reduced by the amount of (time-dependent) strain occurring after the maximum stress is reached, the difference between simulated and measured ratchetting behaviour becomes significantly smaller.

6 Conclusion

In the present study, the cyclic elastic-plastic material behaviour of thin electrical steel sheets has been described with the combined isotropic-kinematic hardening model according to Lemaitre and Chaboche. For the calibration, isotropic and kinematic hardening material parameters have to be determined based on symmetric strain-controlled cyclic tests. Special considerations regarding the test setup are required to prevent buckling of the 0.27 mm thin steel sheets. Using a coated anti-buckling device, representative tests can be performed for strain amplitudes until 0.6 %. The calibration of the kinematic hardening component showed that the back stress α is accurately described by a parameter set (C_i, γ_i) consisting of three components.

The isotropic hardening component has to account for different slopes in the evolution of the yield surface size to capture both the monotonic behaviour in the first half cycle and the subsequent cyclic behaviour. With the proposed multilinear approach, the yield plateau (initial cyclic softening) is described as difference between the experimentally determined stress-strain relation of the first half cycle and the kinematic hardening component. After that, the cyclic hardening is represented by the calculated data pairs (σ_i^0, $\bar{\varepsilon}_i^{\mathrm{pl}}$) starting from the second cycle.

The comparison of numerical simulations with cyclic tests under strain-control showed a good alignment with respect to the shape of the predicted stress-strain hysteresis curves. The yield plateau as well as the onset of cyclic hardening can be appropriately captured. However, the influence of time-dependent plastic deformation cannot be considered which results in noticeable deviations for small strain ranges and the underestimation of the ratchetting behaviour under stress-control. Based on the presented results, the calibrated combined isotropic-kinematic hardening model can be used in further works to assess the fatigue life of electrical steel sheets under proportional cyclic loading.

Acknowledgements

This study was performed as part of the research project “Schwingfestes Elektroblech” funded by the Federal Ministry of Education and Research (BMBF) and the Audi AG. The present work was developed at the Technische Hochschule Ingolstadt in cooperation with the Otto-von-Guericke-Uni-

© 2022 The Authors. Materialwissenschaft und Werkstofftechnik published by Wiley-VCH GmbH

versität Magdeburg. Open access funding enabled and organized by Projekt DEAL.

7 References

[1] R. Halama, J. Sedlák, M. Šofer, in *Numerical Modelling*, (Ed: P. Miidla), IntechOpen, London **2012**, pp. 329–354.
[2] J.S. Novak, D. Benasciutti, F. De Bona, A. Stanojević, A. DeLuca, Y. Raffaglio, *IOP Conf. Ser.: Mater. Sci. Eng.* **2016**, *119*, 012020.
[3] J. Lemaitre, J.-L. Chaboche, *Mechanics of Solid Materials*, Cambridge University Press, Cambridge **2000**.
[4] C.I. Zub, A. Stratan, D. Dubina, *ITM Web Conf.* **2019**, *29*, 02011.
[5] J.S. Novak, F. De Bona, D. Benasciutti, *Metals* **2019**, *9*, 950.
[6] J.-L. Chaboche, *Int. J. Plast.* **2008**, *24*, 1642.
[7] Dassault Systèmes Simulia Corp., Abaqus Documentation 2020: Models for metals subjected to cyclic loading **2020**, Dassault Systèmes, France.
[8] P.J. Armstrong, C.O. Frederick, *CEGB Cent. Electr. Gener. Board*, *Report RD/B/N731*, Berkley, UK, **1966**.
[9] W. Prager, *J. Appl. Phys.* **1949**, *20*, 235.
[10] J.-L. Chaboche, K. Dang Van, G. Cordier, presented at *5th Int. Conf. Struct. Mech. React. Technol.* Berlin, Germany, **1979**, Report number L11/3, pp. 1–10.
[11] J.-L. Chaboche, G. Rousselier, *J. Pressure Vessel Technol.* **1983**, *105*, 153.
[12] J.-L. Chaboche, *Int. J. Plast.* **1986**, *2*, 149.
[13] E. Voce, *Metallurgia* **1955**, *41*, 219.
[14] K.H. Nip, L. Gardner, C.M. Davies, A.Y. Elghazouli, *J. Constr. Steel Res.* **2010**, *66*, 96.
[15] E. Arslan, W. Mack, M. Zigo, G. Kepplinger, *PAMM Proc. Appl. Math. Mech.* **2017**, *17*, 385.
[16] B. Paygozar, S.A. Dizaji, M.A. Saeimi Sadigh, *J. Mech. Eng. Sci. (JMES)* **2020**, *14*, 6848.
[17] H.-J. Christ, Wechselverformung von Metallen: Zyklisches Spannungs-Dehnungs-Verhalten und Mikrostruktur, Springer, Berlin, Heidelberg **1991**.

Received in final form: February 15th 2022

© 2022 The Authors. Materialwissenschaft und Werkstofftechnik published by Wiley-VCH GmbH